Universiteit Leiden
The Netherlands

In uveal melanoma G alpha-protein GNA11 mutations convey a shorter disease-specific survival and are more strongly associated with loss of BAP1 and chromosomal alterations than G alpha-protein GNAQ mutations

Piaggio, F.; Croce, M.; Reggiani, F.; Monti, P.; Bernardi, C.; Ambrosio, M.; ... ; Amaro, A.

Citation
Piaggio, F., Croce, M., Reggiani, F., Monti, P., Bernardi, C., Ambrosio, M., ... Amaro, A. (2022). In uveal melanoma G alpha-protein GNA11 mutations convey a shorter disease-specific survival and are more strongly associated with loss of BAP1 and chromosomal alterations than G alpha-protein GNAQ mutations. *European Journal Of Cancer*, *170*, 27-41. doi:10.1016/j.ejca.2022.04.013

Version: Publisher's Version
License: Leiden University Non-exclusive license
Downloaded from: https://hdl.handle.net/1887/3485613

Note: To cite this publication please use the final published version (if applicable).

European Journal of Cancer 170 (2022) 27–41

Available online at www.sciencedirect.com

ScienceDirect

journal homepage: www.ejcancer.com

Original Research

In uveal melanoma Gα-protein GNA11 mutations convey a shorter disease-specific survival and are more strongly associated with loss of BAP1 and chromosomal alterations than Gα-protein GNAQ mutations

Francesca Piaggio [a], Michela Croce [a], Francesco Reggiani [a], Paola Monti [a], Cinzia Bernardi [a], Marianna Ambrosio [a], Barbara Banelli [a], Mehmet Dogrusöz [b], Ralf Jockers [c], Domenico Bordo [a,1], Roberto Puzone [a,1], Silvia Viaggi [d,e], Domenico Coviello [d], Francesco B. Lanza [f], Martina Bartolucci [g], Andrea Petretto [g], Carlo Mosci [h], Rosaria Gangemi [a], Pieter A. van der Velden [b], Martine J. Jager [b], Ulrich Pfeffer [a,*], Adriana Amaro [a]

[a] *IRCCS Ospedale Policlinico San Martino, Genova, Italy*
[b] *Department of Ophthalmology, Leiden University Medical Center, Leiden, the Netherlands*
[c] *Université de Paris, Institut Cochin, INSERM, CNRS, F-75014 PARIS, France*
[d] *Laboratorio Genetica Umana, IRCCS Istituto Giannina Gaslini, IRCCS Giannina Gaslini Institute Genova, Italy*
[e] *Department of Earth Sciences, Environment, and Life, Università Degli Studi di Genova, Genova, Italy*
[f] *Ocular Oncology Service, Department of Surgical Oncology, Fondazione IRCCS Istituto Nazionale Dei Tumori, Via Venezian 1, 20133 Milan, Italy*
[g] *Core Facilities-Clinical Proteomics and Metabolomics, IRCCS Giannina Gaslini Institute, Genova, Italy*
[h] *Ente Ospedaliero Galliera, Genova, Italy*

Received 13 January 2022; received in revised form 8 March 2022; accepted 4 April 2022
Available online 14 May 2022

KEYWORDS
Uveal melanoma;
G-protein;
DNA methylation;
Metastasis;
Tandem affinity

Abstract ***Background and aim of the study:*** Mutations in the Gα-genes *GNAQ* and *GNA11* are found in 85–90% of uveal melanomas (UM). Aim of the study is to understand whether the mutations in both genes differentially affect tumor characteristics and outcome and if so, to identify potential mechanisms.
Methods: We analyzed the association between *GNAQ* and *GNA11* mutations with disease-specific survival, gene expression profiles, and cytogenetic alterations in 219 UMs. We used

* *Corresponding author*. Tumor Epigenetics Unit, IRCCS Ospedale Policlinico San Martino, Largo Rosanna Benzi 10, 16132 Genova, Italy.
E-mail address: ulrich.pfeffer@hsanmartino.it (U. Pfeffer).
[1] These colleagues have retired.

https://doi.org/10.1016/j.ejca.2022.04.013
0959-8049/© 2022 Elsevier Ltd. All rights reserved.

purification;
Mass spectrometry

tandem-affinity-purification, mass spectrometry and immunoprecipitation to identify protein interaction partners of the two G-proteins and analyzed their impact on DNA-methylation.
Results: *GNA11* mutation was associated with: i) an increased frequency of loss of *BRCA1*-associated protein 1 (*BAP1*) expression ($p = 0.0005$), ii) monosomy of chromosome 3 ($p < 0.001$), iii) amplification of chr8q ($p = 0.038$), iv) the combination of the latter two ($p = 0.0002$), and inversely with v) chr6p gain ($p = 0.003$). Our analysis also showed a shorter disease-specific survival of *GNA11*-mutated cases as compared to those carrying a *GNAQ* mutation (HR = 1.97 [95%CI 1.12–3.46], $p = 0.02$). GNAQ and GNA11 encoded G-proteins have different protein interaction partners. Specifically, the Tet Methylcytosine Dioxygenase 2 (*TET2*), a protein that is involved in DNA demethylation, physically interacts with the *GNAQ* protein but not with *GNA11*, as confirmed by immunoprecipitation analyses. High-risk UM cases show a clearly different DNA-methylation pattern, suggesting that a different regulation of DNA methylation by the two G-proteins might convey a different risk of progression.
Conclusions: GNA11 mutated uveal melanoma has worse prognosis and is associated with high risk cytogenetic, mutational and molecular tumor characteristics that might be determined at least in part by differential DNA-methylation.
© 2022 Elsevier Ltd. All rights reserved.

1. Introduction

Approximately 5% of all melanomas affect the eye [1]. The incidence of uveal melanoma (UM) in the USA is 4.3 per million (4.1–4.5; 95% confidence interval) [2]. The European Cancer Registry-based study on survival and care of cancer patients (EUROCARE) for the years 1983–1994 reported similar incidence rates, with a characteristic increase from south to north, from <2 per million in Spain and southern Italy to >8 per million in Norway and Denmark [3]. Despite successful local treatment, many UM patients develop metastases: 25% and 34% within 5 and 10 years, respectively. Median survival after diagnosis of metastatic UM is approximately one year [4]. The long-term cumulative uveal melanoma-related mortality rate is over 50% for medium and large tumors at 25 years after primary treatment [5]. For recent reviews see Refs. [6–8].

Mutations in *GNAQ* [9] and *GNA11* [10], two genes encoding Gα subunits of G-proteins, are considered drivers of UM carcinogenesis. These mutations are present in 7% of blue nevi and are found in a mutually exclusive manner in most UMs [6,11,12]. Three cases with mutations in both genes have been reported [13,14]. Mutations occur in two hotspot codons i.e., Gln 209 and, less frequently, Arg183, both located in the Ras-like GTPase domain of the protein [15]. The G-proteins, *GNAQ* and *GNA11,* activate the G-protein signaling cascade [16] and the organ size control-associated transcription factor complex *YAP/TAZ* [17,18].

Two reports have described a significantly increased frequency of *GNA11* mutations in metastatic UM: Van Raamsdonk *et al.* reported mutations of *GNA11* and *GNAQ* in 56.5% (n = 13) and 21.7% (n = 5) of patients respectively [10] and Griewank *et al.* found 60% (n = 18) *GNA11* versus 20% (n = 6) *GNAQ* mutations [19]. UM patients with *GNA11* mutations had significantly reduced survival [19]. In another study of 85 *GNAQ* or *GNA11* mutated UM, *GNA11* showed no difference in disease-free survival with a trend towards more rapid development of metastases. A recent analysis showed a trend towards an increased incidence of metastases in *GNA11* mutated UM as compared to *GNAQ* mutated cases that did, however, not reach significance [20]. Here we analyze the association of *GNAQ* and *GNA11* mutations with metastatic UM in three cohorts of a total of 219 cases with known mutation status. For most of these cases, cytogenetic, gene expression, and follow-up data were available.

2. Results

2.1. Structural similarity of GNAQ and GNA11 proteins

Alignment of the protein sequences of *GNAQ* and *GNA11* reveals an identity of 90%. Both proteins are composed of two lobes, a *RAS*-like domain and a second domain consisting of a six-helix bundle. The nucleotide-binding domain is located between the two lobes. The differences in amino acid composition are mostly concentrated in the helical domain (22 out of 28 substitutions in *GNAQ* versus *GNA11*, Fig. 1). Notably, all the mutated residues, except Glu95Asp, are located in positions not involved in the quaternary structure formation with the β and γ subunits [as inferred from the structure of the homologous *Rattus norvegicus GNAI1* alpha1 (GDP) β1 γ1 heterotrimer (Protein Data Bank entry 1GG2)] [21]. These sequence variations between *GNAQ* and *GNA11* are likely to affect the

Fig. 1. Sequence variation between *GNAQ* and *GNA11* proteins. A) Ribbon representation of the model of the *GNA11* molecule built by homology on the crystallographic structure of the murine *GNAQ* used as template [43]. The first 37 amino acids are not shown as they are disordered in the template structure. The six-helix bundle domain is in the upper part of the picture, the *RAS*-like domain in the lower one. The bound GTP molecule is shown in ball-and-stick. B) Positions of conservative and non-conservative amino acid differences between *GNA11* and *GNAQ* are colored in blue and orange, respectively. Arg183 and Gln209 side chains are shown in magenta; Ile62, Val179, and Phe339 side chains are colored in yellow. The nucleotide-binding amino acid stretches dubbed G-1 – G-5 boxes [19] are shown in green. (For interpretation of the references to colour in this figure legend, the reader is referred to the Web version of this article.)

interactions with other proteins that are mediated by the helical domain (for further details see Supplement 1).

2.2. Comparison of *GNAQ* and *GNA11* gene expression in relationship with their mutational status

We analyzed three cohorts of primary UM for a total of 276 cases (124 from the Department of Ophthalmology, Leiden University Medical Center, Leiden, The Netherlands [22]), 72 from the Laboratory of Tumor Epigenetics, Ospedale Policlinico San Martino, Genoa, Italy [23,24] and 80 from TCGA-UVM) [25]. For 258 of these cases *GNAQ* and *GNA11* mutational status, other somatic mutations, cytogenetic alterations, and clinical follow-up were available. *GNAQ* and *GNA11* mutations were mutually exclusive in all except two cases of the TCGA cohort. Double mutant and double wild type cases were not considered in this study resulting in a dataset of 219 UM patients. For 190 of them, *GNAQ* and not recursive *GNA11* expression profiles were available. Patient characteristics and their associations with *GNAQ* or *GNA11* mutation status are reported in Table 1.

Different effects of mutations in the two G-proteins could be determined by different expression levels, since activating mutations in a more highly-expressed gene are expected to elicit stronger effects on signaling. We observed a slightly higher expression of *GNA11* than *GNAQ* in the gene expression profiles of the combined dataset of 190 UM cases that was cleaned from batch effects, as previously described (Suppl. Figure 1a). The mRNA expression of the two G-proteins was not significantly different in UMs carrying *GNAQ* or *GNA11* mutations and the presence of the mutation does not induce an increased expression of the corresponding G-protein compared to the wild type protein (Suppl. Fig. 1b–c).

2.3. Association of *GNAQ* and *GNA11* mutations with cytogenetic features and BAP1 mutations

Prior reports on survival concerning GNA11 and GNAQ have provided contradictory results. Such reports concerned small series [10,19]. We therefore analyzed the association of *GNAQ* and *GNA11* mutations with survival and cytogenetic alterations in a cohort of 219 patients. In Kaplan–Meier analysis for disease-specific survival GNA11 mutated cases showed a shorter disease specific survival (HR = 2.02 [95% CI 1.13–3.62], p = 0.014) (Fig. 2). The hazard ratio (univariate Cox) for disease-specific death of a *GNA11* vs *GNAQ* mutation was HR = 1.97 [95% CI 1.12–3.46], (p = 0.02). The association of *GNA11* mutations with survival had a similar trend in all three cohorts (Supp. Figure 2).

Fifty-one of 107 primary UM cases (48%) with a *GNA11* mutation and 43 of 112 cases (38%) with a *GNAQ* mutation developed metastases during follow-up (HR = 1.46 [95% CI 0.85–2.50]). This trend was observed in each of the three cohorts (Table 1) but reached significance neither in the combined (p = 0.17) nor in the single cohorts (data not shown).

Table 1
Patient and sample characteristics.

Data Element	GNAQ		GNA11		Total	Hazard Ratio* [CI]	Significance	
							p-value	Chi-Square
# of cases								
Total	112 (51.14%)		107 (48.86%)		219		0.82	0.398
Leiden	57 (49.14%)		59 (50.86%)		116			
TCGA	38 (53.52%)		33 (46.48%)		71			
Genoa	17 (53.12%)		15 (46.88%)		32			
Age (years)	**median [95% CI]**	**range**	**median [95% CI]**	**range**				
	60 [56.87–62.05]	(27–87)	62.72 [58.41–64.21]	(13–88)			0.35	
Sex								
Male	68 (53.13%)		60 (46.87%)		128		0.49	0.485
Female	44 (48.35%)		47 (51.65%)		91			
Histology n = 218								
Spindle cell	37 (53.62%)		32 (46.38%)		69		0.31	2.339
Epitheloid	16 (40%)		24 (60%)		40			
Mixed	58 (53.21)		51 (46.79%)		109			
Tumor dimensions	**median [95% CI]**	**range**	**median [95% CI]**					
n = 207 largest diameter	15 [13.80–15.39]	(2–30)	14 [13.33–14.99]	(2–25)			0.45	
n = 215 thickness	9 [7.98–9.14]	(1–15)	9 [7.93–9.28]	(1–16)			0.92	
Stage n = 210								
I a-d	6 (37.5%)		10 (62.5%)		16		0.63	1.729
II a-d	29 (48.33%)		31 (51.67%)		60			
III a-d	51 (54.26%)		43 (45.74%)		94			
IV a-e	20 (50%)		20 (50%)		40			
Cytogenetics								
chr3 monosomy n = 204	41 (+2 LOH) (38.68%)		65 (+4 LOH) (61.32%)		106	**2.97 [1.66–5.31]**	**0.0002**	**13.881**
chr8q amplification n = 199	57 (45.6%)		68 (54.4%)		125	**1.85 [1.03–3.32]**	**0.038**	**4.305**
chr3 mon./chr8q amp. n = 193	33 (37.08%)		56 (62.92%)		89	**3.07 [1.71–5.53]**	**0.0002**	**14.363**
chr6p gain n = 199	52 (64.20%)		29 (35.80%)		81	**2.44 [1.36–4.37]**	**0.003**	**9.157**
BAP1 Alteration$ n = 219								
	27		50		77	**2.76 [1.55–4.91]**	**0.0005**	**12.284**
Follow-up (months)	**median [95% CI]**	**Range**	**median [95% CI]**	**range**				
	47.23 [54–72.92]	(0–222)	38.05 [46.96–67.02]	(0–209)			0.35	
Metastases								
Total	43 (45.75%)		51 (54.25%)		94		0.17	1.920
Disease specific death								
	31 (40.26%)		46 (59.74%)		77	**1.97 [1.12–3.46]**	**0.02**	**5.628**
Overall survival n = 77	**median [95% CI]**	**Range**	**median [95% CI]**	**range**				
	31.5 [30.97–53.51]	(2–120)	26.97 [25.02–37.08]	(1–97)			0.058	

Histopathological, cytogenetic, and molecular features of *GNA11* and *GNAQ* mutated primary UM.
The Hazard Ratio is calculated for *GNA11* mutated cases in comparison to *GNAQ* mutated cases. Significant data are reported in bold characters.
* =GNA11 versus GNAQ, $ = for the Leiden cohort, a negative IHC staining was used as surrogate for BAP1 mutation.

GNA11 mutations were not associated with tumor stage but were strongly correlated with cytogenetic alterations like monosomy of chr3 ($p < 0.001$) and amplification of chr8q ($p = 0.038$) (Table 1), both of which are known to be associated with an increased metastatic risk. *GNA11* mutations were inversely associated with gain of chr6p ($p = 0.003$) that has been associated with a more benign behavior of the tumor. *GNA11* mutations also occur significantly more frequently in tumors with both chr3 monosomy and chr8q amplification ($p < 0.001$).

The trend for an association of *GNA11* mutations with metastasis can, at least in part, be explained by the fact that *GNA11*-mutated cases showed a higher frequency of loss of *BAP1* than *GNAQ*-mutated cases (HR 2.76 [95% CI = 1.55–4.91], $p < 0.001$, Table 1). For the analysis of BAP1, we used mutation data from the TCGA and the Genoa cohort (103 UM) and immunohistochemistry data from the Leiden cohort (116 UM) since BAP1 mutations abolish the expression of the protein in the nuclei of the cells [13,26–30].

Of the 51 metastatic UM patients with GNA11 mutations, 46 (90.19%) died within the period of observation. Twenty-nine (63.04%) of these carried a BAP1 mutation. Thirty-one (72.09%) of 43 metastatic patients with GNAQ mutations died and 16 (51.61%) of them carried a BAP1 mutation (HR = 3.25 [95% CI 1.46–7.22], $p = 0.03$). *GNA11* mutations were not associated with the thickness and the largest diameter of the primary tumor, age at diagnosis, sex, and histology; Table 1).

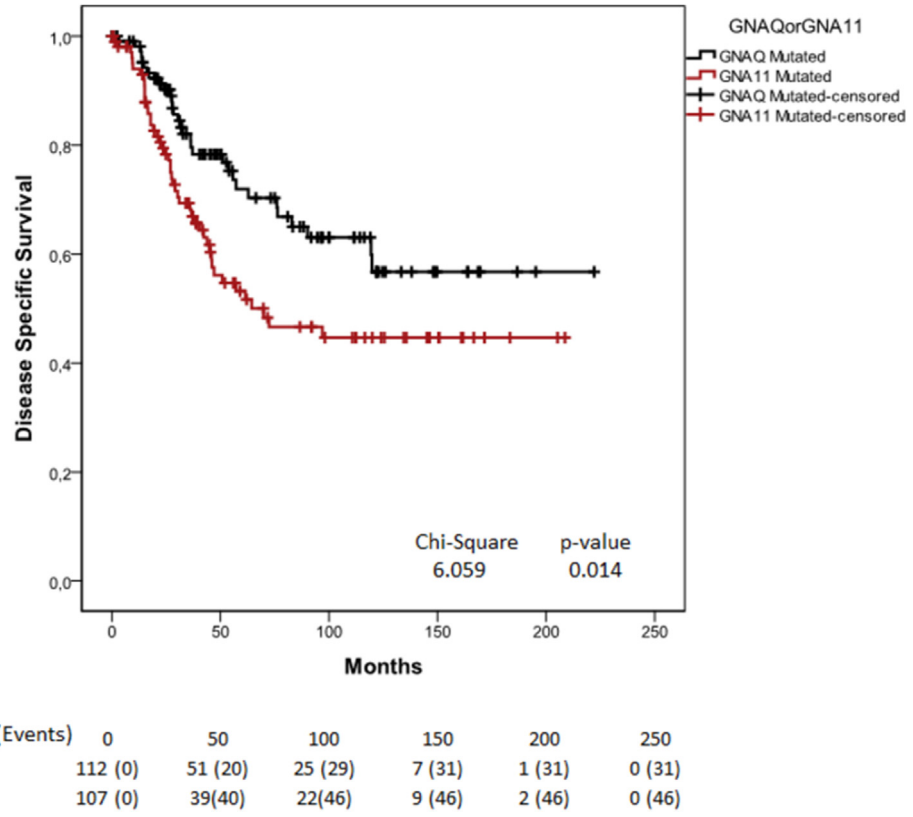

Fig. 2. Kaplan–Meier disease-specific survival analysis on Cox proportional hazard multiple regression model for *GNAQ* and *GNA11* mutated primary UMs. *GNA11* mutated cases showed a more rapid progression towards the death of disease (HR = 2.02 [95% CI 1.13–3.62], p = 0.014).

Table 2
Estimation of infiltrating cells and tumor purity by gene expression data analysis.

MCP	GNAQ		GNA11		Chi-Square	p-value	Odds Ratio	95% Interval Confidence	
	Low	High	Low	High				Lower	Upper
T cells	48	28	32	47	**7.958**	**0.005**	**2.518**	**1.318**	**4.810136**
CD8 T cells	48	28	31	48	**8.867**	**0.003**	**2.654**	**1.387**	**5.079**
Cytotoxic lymphocytes	40	36	39	40	0.165	0.684	1.14	0.607	2.14
NK cells	41	35	39	40	0.325	0.568	1.201	0.639	2.258
B lineage	33	43	46	33	3.398	0.065	0.551	0.291	1.041
Monocytic lineage	42	34	39	40	0.54	0.463	1.267	0.674	2.383
Myeloid dendriticcells	40	36	40	39	0.062	0.803	1.083	0.577	2.035
Neutrophils	42	34	39	40	0.54	0.463	1.267	0.674	2.383
Endothelial cells	34	42	43	36	1.456	0.228	0.678	0.36	1.276
Fibroblasts	40	36	40	39	0.62	0.803	1.083	0.577	2.035

Identification and qualitative validation of transcriptomic markers of stromal and immune infiltrated cells obtained from MCPcounter algorithm concerning GNAQ or GNA11 mutated UMs. Significant data are reported in bold characters.

2.4. Differential gene expression in GNAQ and GNA11 mutated UMs

We investigated if *GNAQ* and *GNA11* mutations were correlated to differences in gene expression that might functionally explain their effects on UM progression. We performed a rigorous class comparison analysis using Significance Analysis of Microarrays on the gene expression profiles of a combined dataset of 190 cases that were cleaned from batch effects, as previously described [31]. Thirty-five genes were differentially expressed in *GNAQ*-versus GNA11-mutated cases in a statistically significant manner (Fig. 3a). Gene enrichment analysis showed their involvement in GTPase activation and regulation of immune response (Fig. 3b). Among the overexpressed genes in *GNA11*-mutated cases, we identified the phospholipase C beta 2 Protein (*PLCB2*), the Signal Transducer and Activator of Transcription 3 (*STAT3*), and the GTPase-Activating Protein (*ASAP1*, also named *DDEF1*). *ASAP1* is involved in the regulation of the interrelated signaling pathways of *GNAQ*/*GNA11*, *RhoA*, *ARF1*, *ARF6,* and Phosphatidylinositol-4,5-

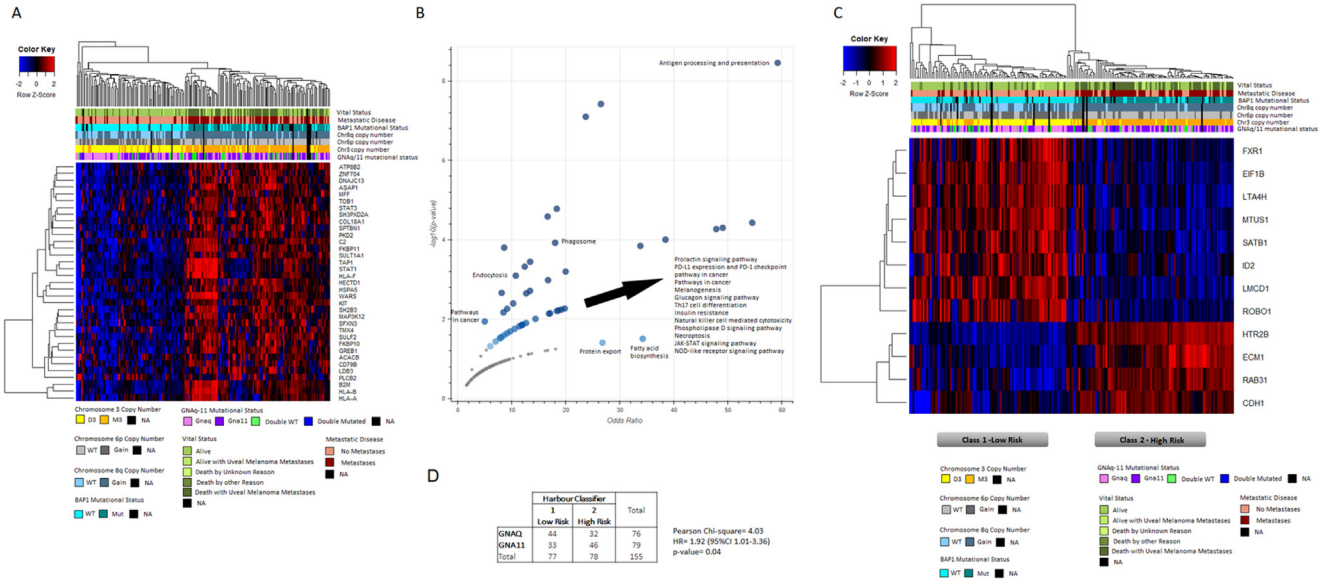

Fig. 3. Gene expression depending on the *GNAQ* and *GNA11* mutational status in UMs. A. The expression profiles of cases with *GNAQ* and *GNA11* mutations were interrogated by Significance Analysis of Microarrays and the expression values of significant genes were clustered by hierarchical clustering. The two clusters formed were enriched for cases with *GNA11* (right cluster) and *GNAQ* (left cluster) mutations. The expression values are reported by a color scale (blue = expression below the mean, red = expression above the mean, black = expression at the mean; the intensity is related to the distance from the mean). The bars above the dendrogram show the mutation status (*GNAQ* mutated = pink, GNA11 mutated = purple, both wild type = green and both mutated = blue), patient status (dark red = metastatic, dark salmon = metastasis-free), death of disease (gradient starting from dark olive green = Death with UM metastases, to light-olive green = Alive), *BAP1* protein expression (turquoise = absent, intense turquoise = present), chr3 status (orange = monosomic, yellow = disomic), chr8q status (intense sky blue = gain, light sky blue = no gain) and chr6p status (dark gray = gain, light gray = no gain). Cases with missing information = black. B. Gene set enrichment analysis for biological pathways to which DEGs analyzed by SAM are annotated. The pathways with the highest confidence levels are shown (https://maayanlab.cloud/Enrichr/). C. Association of *GNAQ* and *GNA11* mutations with prognostic molecular classes. The gene expression-based prognostic classifier was used for hierarchical clustering of UM cases with *GNAQ* and *GNA11* mutations. The expression values are reported as above stated. D. Contingency table of *GNAQ* and *GNA11* mutated cases concerning stratification by Harbour multigene classifier. *GNA11* mutated patients showed a more enrichment in high risk class 2 group (HR = 1.92 [95% CI 1.01−3.36], p = 0.04). (For interpretation of the references to colour in this figure legend, the reader is referred to the Web version of this article.)

Bisphosphate 3-Kinase (*PI3K*); *PLCB2*, an orthologue of the UM driver gene *PLCB4*, has been previously proposed as a secondary driver [31]. Supplementary Table 1 shows the list of differentially expressed genes and supplementary Table 2 indicates the related gene enrichment analysis for biological pathways.

We applied the molecular classifier developed by Harbour and colleagues [32] to the expression data of the 190 Ums. The analysis showed that the cluster of class 1 cases with low risk of metastasis had prevalently *GNAQ* mutations whereas most of *GNA11* mutated UM fell in the cluster of class 2, associated to high metastatic risk. Fourty-four (57.9%) of 76 *GNAQ*-mutated UMs belong to the low-risk class 1 and 32 (42.1%) to the high-risk class 2 while 33 (41.8%) of 79 *GNA11*-mutated cases were classified to class 1 and 46 (58.2%) to class 2 (HR = 1.92 [95% CI 1.01−3.36], p = 0.04) (Fig. 3d). The associations with specific cytogenetic features (monosomy of chr3, amplification of chr8q, and, inversely, chr6p gain) and BAP1 mutation are also *evident* (Fig. 3c).

It is known that class two (poor prognosis) UM patients are characterized by greater tumor infiltrate, so we analyzed the composition of tumor infiltrate for 190 primary UMs using the MCPcounter tool [webMCP-counter: a web interface for transcriptomics-based quantification of immune and stromal cells in heterogeneous human or murine samples [62,63,64]. We found a significant increase of T cells and CD8 T cells in GNA11 mutated patients (Table 2).

2.5. Differential gene expression in accordance to GNAQ and GNA11 mutational status in UM cell lines

The association of an increased metastatic risk with *GNA11* mutations could also rely on the effects of the immune infiltrate on global gene expression variation. To assess the effects of *GNAQ* and *GNA11* mutations on different signaling pathways in the absence of immune cells, we decided to perform differential gene expression analyses on a panel of eight UM cell lines with or

without *GNAQ* and *GNA11* mutations (MEL285 and MEL290, wild type; OMM1, UPMD1 and UPMD2, *GNA11* only mutated; UPMM1, UPMM2 and UPMM3 only *GNAQ* mutated). Very few viable UM cell lines show chr3 monosomy and, unfortunately, our collection of cell lines does not reflect the association of *GNA11* mutations with chr3 monosomy.

The gene expression profiles of *GNAQ* and *GNA11*-mutated cells were evaluated by class comparison analysis, through SAM analysis, showing that 118 genes were differentially expressed, in a statistically significant manner, in *GNAQ* versus *GNA11*-mutated cell lines (106 up-regulated and 12 down-regulated) (Fig. 4a). The gene enrichment analysis of differentially expressed genes showed that these genes are significantly involved in the signaling of phospholipase D and Rap1 and the pathways involving epithelial–mesenchymal transition (EMT) and focal adhesion (Fig. 4b). The list of differentially-expressed genes in the cell lines and the gene enrichment analysis for biological pathways are shown in supplementary Tables 3 and 4, respectively. Genes differentially expressed in cell lines show only a minimal overlap with genes differentially expressed in human tumors, which is likely since the latter often reflects the tumor infiltrate.

2.6. Different interactions partners of GNAQ and GNA11 proteins identified by tandem affinity purification and mass spectrometry (TAP-MS/MS) analysis

Functional differences between the two G-proteins might be determined by different interaction partners. To investigate this aspect, we employed Tandem Affinity Purification and Mass Spectrometry (TAP-MS/MS) [33] to identify proteins that interact with *GNAQ* or *GNA11*. Specifically, we decided to transfect the OMM1 *GNA11* mutated cell line with four different constructs carrying the mutated or wild type form of both G-protein genes or with the vector alone, as a negative control. Western blot analysis confirmed the expression of *GNAQ* and *GNA11* proteins in cells transfected with the corresponding constructs, indicating its efficient intracellular delivery (Suppl. Figure 3).

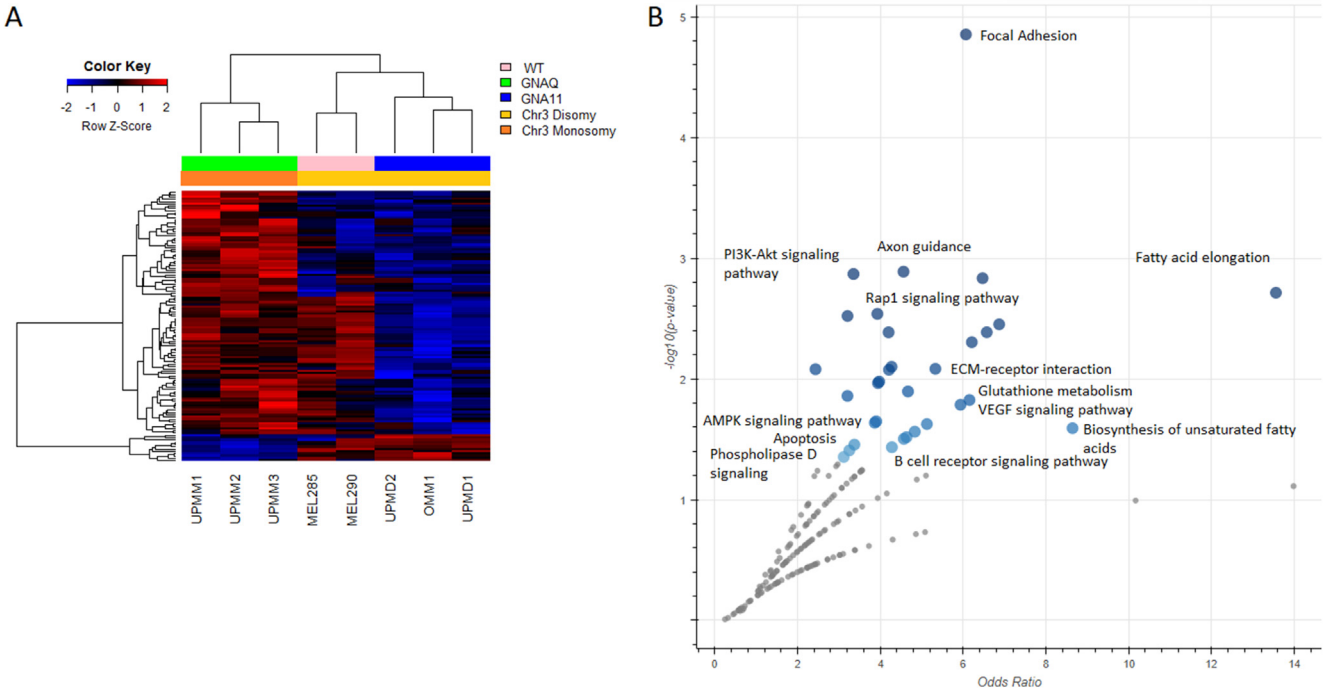

Fig. 4. Differential gene expression related to the *GNAQ* and *GNA11* mutational status in UM cell lines. A) The expression profiles of *GNAQ* and *GNA11* mutated cell lines were interrogated by Significance Analysis of Microarrays and the expression values of significant genes were clustered by hierarchical clustering. The expression values are reported by a color scale (blue = expression below the mean, red = expression above the mean, black = expression at the mean; the intensity is related to the distance from the mean). The bars above the dendrogram show the expression status (*GNAQ* mutated = green, *GNA11* mutated = slate blue, both wild type = pink), chr3 status (orange = monosomic, yellow = disomic). B) Gene set enrichment analysis for biological pathways to which DEGs analyzed by SAM are annotated (https://maayanlab.cloud/Enrichr/). The plot shows the significance of each gene set from the selected gene ontology vs its odds ratio. Each point represents a single gene set; the x-axis measures the odds ratio (0, inf) calculated for the gene set, while the y-axis gives the -log (p-value) of the gene set. Larger blue points represent significant terms (p-value < 0.05); smaller gray points represent non-significant terms. The darker the blue color of a point, the more significant it is. (For interpretation of the references to colour in this figure legend, the reader is referred to the Web version of this article.)

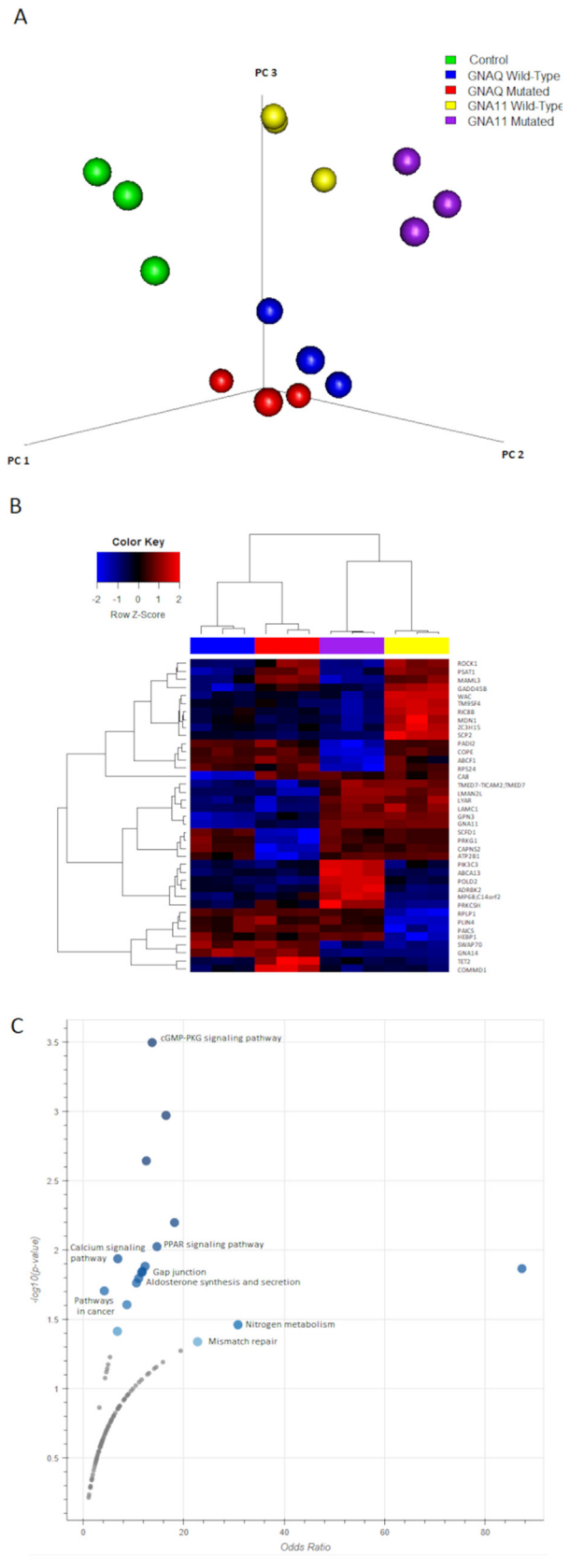

Fig. 5. *GNAQ* and *GNA11* protein interaction partners in OMM1 cell lines. A) Three-dimensional scatter plot of the principal component analysis of *GNAQ* wild type (blue dots), *GNA11* wild type (yellow dots), *GNAQ* mutated (red dots), -*GNA11* mutated (purple dots), and control (green dots). B) Unsupervised hierarchical-clustered heatmap of *GNAQ* and *GNA11* protein interaction partners. The heatmap shows relative intensity values of proteins identified through Tandem-Affinity-Purification/ Mass Spectroscopy. Proteins differentially interacting with *GNAQ* and *GNA11* in cell lines expressing mutated or non-mutated transgenic G proteins were analyzed by multiclass SAM and significant interaction differences were clustered by hierarchical clustering. Relative intensities are reported by a color scale (blue = intensity below the mean, red = intensity above the mean, black = intensity at the mean; the color-intensity is related to the distance from the mean). The bars above the dendrogram show the transfected G-protein constructs (*GNAQ* wild type = blue, *GNAQ* mutated = red, *GNA11* wild type = yellow, and *GNA11* mutated = purple). C) Gene set enrichment analysis for biological pathways for which differentially interacting proteins are annotated (https://maayanlab.cloud/Enrichr/). The plot shows the significance of each gene set from the selected gene ontology versus its odds ratio. Each point represents a single gene set; the x-axis measures the odds ratio (0, inf) calculated for the gene set, while the y-axis gives the -log (p-value) of the gene set. Larger blue points represent significant terms (p-value < 0.05); smaller gray points represent non-significant terms. The darker the blue color of a point, the more significant it is. (For interpretation of the references to colour in this figure legend, the reader is referred to the Web version of this article.)

Interaction partners were captured by affinity purification via the two protein tags added N-terminally in frame to the coding sequences of *GNAQ* and *GNA11* and identified by mass spectrometry analysis of the peptides obtained after enzymatic digestion of the captured proteins. A principal component analysis of the identified interaction partners showed limited variation in each experimental group and extensive differences between groups (Fig. 5a). All G-protein baits yielded a pattern of interaction partners clearly distinct from that observed using the void control vector (green dots) and *GNAQ* and *GNA11* baits generated fairly distant patterns. The mutated form of *GNAQ* showed a pattern that was only slightly different from the pattern associated with the wild type bait whereas the *GNA11* mutated form showed a more clearly separated pattern when compared to its wild type counterpart (Fig. 5a). These differences are highlighted by the analysis of the interaction partners by bootstrapping statistics. The multiclass SAM analysis shows 39 interaction partners (Fig. 5b and Suppl. Table 5). While proteins involved in the cyclic guanosine monophosphate/CGMP-Dependent Protein Kinase (c-GMP-PKG) and the c-AMP signaling pathways are enriched among the interaction partners of the mutated *GNAQ*, the Peroxisome Proliferator-Activated Receptor (PPAR) signaling pathway is enriched in mutated *GNA11* (Fig. 5c, Suppl. Table 6).

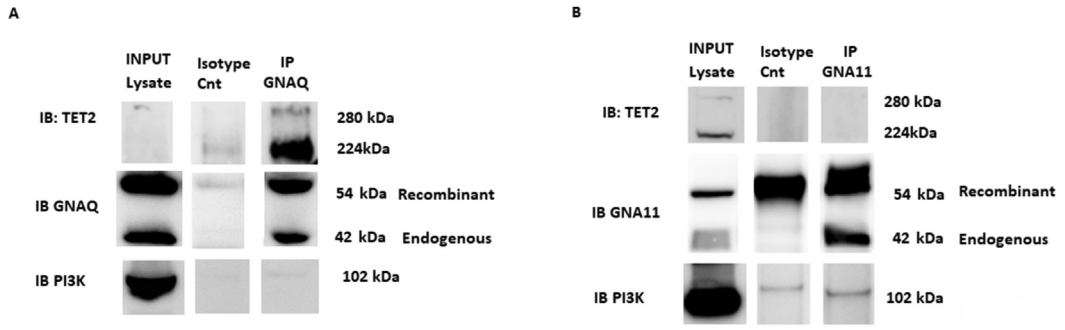

Figure: 6. CO-Immunoprecipitation assay in OMM1 cell lines. The mutated forms of *GNAQ* or *GNA11* were transfected into OMM1 cells. Immunoprecipitations were performed using total cell lysates either with anti-*GNAQ* (A) or *GNA11* (B) antibodies followed by immunoblot analysis using an anti-*TET2* antibody (A, B) (first row), anti-*GNAQ* (A), anti-*GNA11* (B) (second row) and anti-PI3K antibodies (third row). Equal amounts of lysates were immunoprecipitated with isotype control antibodies (middle lane).

2.7. Analysis of interactions partners of GNAQ and GNA11 proteins by Co-Immunoprecipitation (Co-IP) analysis

We then decided to test two of the main interactors identified above, one for each G-protein, by conventional immunoprecipitation analysis in OMM1 cell line transfected with a mutated form of *GNAQ* and *GNA11* proteins. Given the striking difference in DNA-methylation between high and low risk UM [14,34], we focused on Tet Methylcytosine Dioxygenase 2 (*TET2*) as an interaction partner of mutated *GNAQ*. Among the interaction partners of mutated *GNA11*, we addressed the oncogene product Phosphatidylinositol-4,5-Bisphosphate 3-Kinase (*PI3K*).

The Western Blot analysis using *TET2* specific antibodies showed that mutated *GNAQ* but not mutated *GNA11* co-immunoprecipitated *TET2* (Fig. 6). A similar analysis did not comfirm PI3K binding to *GNA11* since the protein was also precipitated using isotype control antibodies.

The interaction of *TET2* with *GNAQ* but not with *GNA1* recursive might determine different DNA-methylation patterns according to the mutational status of UMs. We, therefore, analyzed the methylation patterns of the samples from the TCGA cohort by comparing cases with *GNAQ* versus *GNA11* mutations by bootstrapping statistics. The analysis showed that 356 genes were differentially methylated in *GNAQ* -vs *GNA11*-mutated cases in a statistically significant manner (217 hypermethylated and 139 hypomethylated genes) (Fig. 7 and Suppl. Table 7). Hierarchical clustering of the TCGA cases using the methylation values of these genes also distinguished chr3 copy number and BAP1 mutational status, the two main prognostic markers of UM.

3. Discussion

Mutations in the G protein *GNAQ* or *GNA11* occur at an early stage of UM carcinogenesis with more than 85% incidence. Growing evidence shows a more aggressive behavior of UMs harboring *GNA11* mutations. Functional differences between *GNAQ* and *GNA11* are also evident from developmental studies. *GNAQ* and *GNA11* have been reported to determine skin color in mice where hypermorphic mutations of these genes are associated with higher pigmentation of the dermis, not the epidermis [35]. It is interesting how *GNAQ* knock-out mice show a lighter colored skin whereas *GNA11* knockouts do not affect skin color, indicating a higher penetrance of the former at least as far as skin color is concerned [35]. *GNAQ* and *GNA11* hypermorphic variants determine the number of melanoblasts in the developing embryo at specific phases of development (before E10.5) probably by determining the number of neural crest cells that differentiate into melanoblasts [35]. This leads to a higher density of melanoblasts in the dermis whereas, in the epidermis of older embryos and adults, the number of melanoblasts is not affected by hypermorphic variants [35].

The high conservation of the sequences of the two Gα-proteins casts some doubt on potential functional divergence. We compared the three-dimensional location of the amino acid residues that are divergent between GNAQ and GNA11 and we observed that they map to the surface of a sub-region that is likely to interact with other proteins but not involved in the quaternary structure formation with the β- and γ-subunits of Gα-proteins, thus likely interfering with non-canonical functions of these G-proteins.

Studies on the relation between *GNA11* and *GNAQ* and prognosis in UM have produced diverse results. Two studies, based on very few cases, found a higher frequency of GNA11 than GNAQ mutations in metastatic UMs [10,19]. Another study with 85 cases [13] observed a more rapid progression towards the death of metastases for cases carrying *GNA11* mutations that, however, did not reach statistical significance.

Here we report on 219 informative cases including three cohorts from Genoa [23,24], Leiden [22], and The Cancer Genome Atlas Research Network [25]. Patients

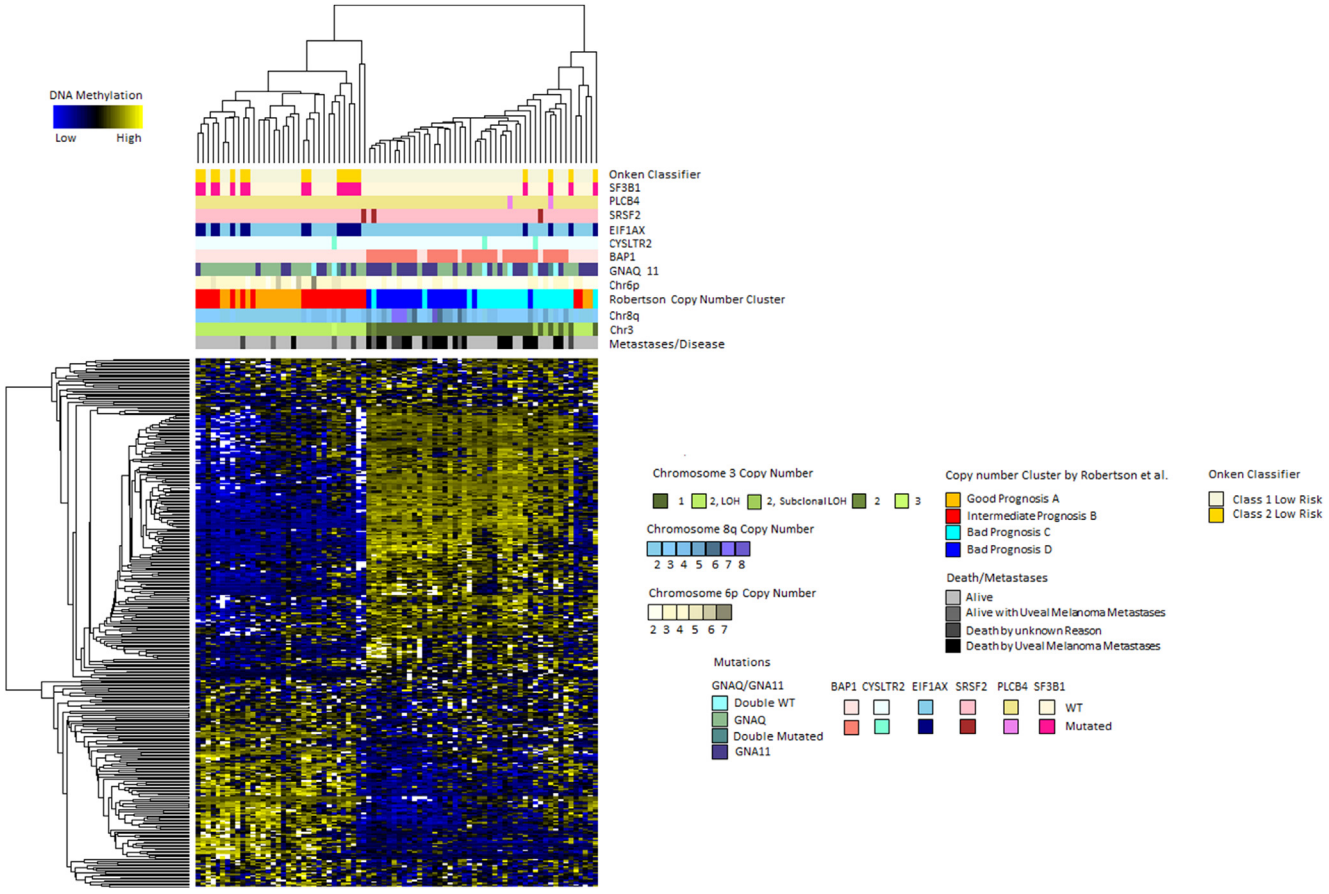

Fig. 7. DNA Methylation Analysis in primary UMs from TCGA dataset. The methylation profiles of cases with *GNAQ* and *GNA11* mutations (TCGA dataset) were interrogated by T-TEST and the methylation levels of significant genes were clustered by hierarchical clustering. The two clusters formed were enriched for cases with *GNA11* (right cluster) and *GNAQ* (left cluster) mutations. The methylation levels are reported by a color scale (blue = methylation below the mean, yellow = methylation above the mean, black = methylation at the mean; the intensity is related to the distance from the mean). The bars above the dendrogram show the Harbour Classifier of metastatic UM risk (Class 1 = beige, Class 2 = gold), the Robertson *et al.* Classifier (Good Prognosis A = orange, Intermediate Prognosis B = red, Bad Prognosis C = cyan, Bad Prognosis D = blue), Death/Metastases (black = Death with UM metastases, light gray = Alive), chr3 status (dark olive green = disomic, light olive green = monosomic), chr8q status (sky blue = no gain, slate blue = gain), chr6p status (ivory = no gain, dark lemon chiffon = gain), *GNAQ* or *GNA11* mutational status (dark slate blue = *GNA11* mutated, dark sea green = *GNAQ* mutated, dark slate gray 1 = both wild-type, dark slate gray 4 = both mutated), *BAP1* protein expression (misty rose = absent, salmon = present), *CYSLTR2* mutational status (azure = wild type, aquamarine = mutated), *EIF1AX* mutational status (sky blue = wild type, navy blue = mutated), *SRSF2* mutational status (pink = wild type, brown = mutated), *PLCB4* mutational status (khaki = wild type, violet = mutated), and *SF3B1* mutational status (corn silk = wild type, deep pink = mutated). (For interpretation of the references to colour in this figure legend, the reader is referred to the Web version of this article.)

with mutations in *GNA11*, compared to those with mutations in *GNAQ*, show a trend towards a higher risk of metastasis that does not reach significance and a significantly increased risk of disease-specific death in a shorter time. The apparently higher potential of *GNA11* mutations to promote tumor progression is likely linked to the association with mutations in the tumor suppressor gene *BAP1* as well as with monosomy of chr3 and amplifications of chr8q and inversely correlates with chr6p gain, four well known prognostic factors [36–39]. *GNA11* mutations are found more frequently in tumors with a class two, high-risk expression profile [32] as compared to *GNAQ* mutations. Since the *GNAQ*/*GNA11* mutations constitute the earliest mutation in UM and predate the loss of a copy of chr3, the type of mutation might directly influence which molecular pathway is triggered [40].

The comparison of the expression profiles of UMs with *GNAQ* and *GNA11* mutations reveal a shortlist of differentially-expressed genes among which we found two genes overexpressed in GNA11-mutated cases that have already been described as involved in UM. Amplification of *ASAP1* has been proposed to explain the effect of chr8q amplification [41] and *PLCB2* is already indicated as a putative secondary driver in UM [31].

The comparison of the protein interaction networks of the two Gα-proteins showed unexpectedly only very

limited overlap, indicating functional differences between *GNAQ* and *GNA11*. The interaction of mutated *GNAQ* with the dioxygenase *TET2*, which is not observed for mutated *GNA11*, was confirmed by co-immunoprecipitation analyses. This interaction is interesting since *TET2* plays an active role in DNA demethylation and high-risk UMs are characterized by widespread demethylation. Remarkably, the list of differentially-methylated genes in *GNAQ*-mutated versus *GNA11*-mutated cases is highly associated with the most important prognostic markers, monosomy of chr3 and *BAP1* mutations.

Our results indicate that there are functional differences between the two Gα-proteins. The specific downstream signaling and the different interaction partners might explain the more aggressive behavior of tumors carrying *GNA11* mutations. A limitation of our study is that we cannot definitely rule out whether the association with the clinical outcome is a direct effect of *GNAQ*/*GNA11* mutations or mediated by other molecular events associated with well-known prognostic markers. Despite the association with prognosis, *GNAQ* and *GNA11* mutations do not reach the prognostic power of established prognostic markers such as BAP1/SF3B1/EIF1AX mutations, chr3 status or class1/class2 gene expression signature.

It is possible that the mutations in the two Gα-proteins also influence drug responses and clinical trials involving metastatic UM should consider the stratification of the responses based on their mutational status. Moreover, the differential methylation observed is expected to be particularly important in the evaluation of epigenetic drugs for the treatment of UM patients.

4. Methods

4.1. Modeling and protein interactions

The three-dimensional model of the human GNA11 molecule has been obtained from the Swiss-Model Repository [42]. The model was built by homology on the crystallographic structure of the murine GNAQ [43] (PDB, 3OHM). As the sequence identity between the two proteins is 90% (324/359 amino acid positions, neither insertions nor deletions in the sequence alignment), the mainchain conformation of the GNA11 protein can be considered reliable. Only minor structural variations are expected as a consequence of mutated residues.

4.2. Datasets

We used data derived from three cohorts of primary UM for a total of 276 cases (124 from the Department of Ophthalmology, Leiden University Medical Center, Leiden, The Netherlands [22]), 72 from the Laboratory of Tumor Epigenetics, Ospedale Policlinico San Martino, Genoa, Italy [23,24] and 80 from TCGA-UVM [14]. For 258 of these cases GNAQ and GNA11 mutational status, somatic mutations, cytogenetic alterations, and clinical follow-up were available. GNAQ and GNA11 mutations were mutually exclusive in all except two cases of the TCGA cohort. Double mutant and double wild type cases were not considered in this study resulting in a dataset of 219 UM patients. For 190 of these samples, gene expression profiles were available (GSE27831, GSE51880, TCGA-UVM). From the Leiden dataset gene expression profiling was carried out on RNA of 64 UMs with Illumina platform as previously described [44]. TCGA-UVM gene expression data were obtained from UCSC-Xenabrowser (http://xena.ucsc.edu/level 3 data, $\log2^{(x+1)}$ transformed RSEM normalized counts).

Gene expression analyses were performed in R. WGCNA and InSilicoMerging packages were used, as previously described [31], to collapse probes to gene symbol to the maximum variance probe set and to merge the three datasets into a single one without batch effects for further analyses. Genomic and copy number analyses were performed as previously described [23,45–47]. GNA11, GNAQ, and BAP1 mutations were detected as described previously [11,48]. Immunohistochemistry was performed as previously described [28].

4.3. Cell lines and microarray

Eight different uveal melanoma cell lines MEL285, MEL290, OMM1 [49,50], UPMM1, UPMM2, UPMM3, UPMD1, and UPMD2 [51] (wild type or specifically mutated for *GNAQ* or *GNA11* as indicated in the main text) were selected as cellular model for the Gα-protein signaling analysis. MEL285 and MEL290 are a gift from Dr. B.R. Ksander, Schepens Eye Research Institute, Boston, USA. OMM1 is a gift from Dr. G.P. M. Luyten, ErasmusMC, Rotterdam, The Netherlands. UPMM1, UPMM2, UPMM3, UPMD1, and UPMD2 are a gift from Dr. Michael Zeschnigk Institute of Human Genetics, University Clinics Essen, University Duisburg-Essen, Essen, Germany. Cell lines were cultured in RPMI 1640 (Gibco-BRL, Rockville, MD, USA) supplemented with 10% fetal bovine serum (FBS), 2 mM L-glutamine, and 100 U/ml penicillin/streptomycin. RNA was extracted from cell lines using RNeasy Plus mini kit (Qiagen, Hilden, Germany). RNA quality was assessed with Nanodrop and Bio-Analyzer tools (Agilent, St. Clara, CA). cDNA, ds-cDNA, and cRNA synthesis and fragmentation were performed using the 3′ IVT Express Kit (Affymetrix, Santa Clara, CA, USA). Hybridization, washing, and staining were performed using the GeneAtlas® (Affymetrix, St. Clara, CA). All microarray data are MIAME compliant. The dataset, corresponding to 8 uveal melanoma cell lines is available from the GEO database (http://www.ncbi.nlm.nih.gov/geo/), under accession number GSE197656.

4.4. TAP-MS/MS

A Tandem Affinity Purification (TAP) followed by double Mass Spectrometry (MS/MS) was performed with the wild type and mutated forms of both GNAQ and GNA11 proteins. V51 pIRES-puroGLUE plasmid (Addgene) containing a HA-tag and two sequences coding for a streptavidin binding protein domain (SBP) and a calmodulin-binding protein domain (CBP) was selected as a backbone for the expression of the wild type (*GNAQ*wt and *GNA11*wt) and mutated forms (*GNAQ*mut and *GNA11*mut). The plasmids are shortly renamed as TAP-*GNAQ*wt, TAP-*GNA11*wt, *GNAQ*-mut, and TAP-*GNA11*mut. The empty backbone indicated as TAP-CTR was also used. The wild type and mutated forms of *GNAQ* and *GNA11* proteins were cloned using a PCR-based method and verified by Sanger sequencing (Bmr Genomics, Padova, Italy). Plasmids were purified using the PureYield Plasmid Midiprep Kit (Promega) according to the manufacturer.

For each condition, four 100 mm Petri dishes of OMM1 UM cells were cultured in 1640 RPMI medium supplemented with 1× NEAA, 1× Pyruvate acid, 2 mM L-glutamine, and 100 U/ml penicillin/streptomycin, and 10% FBS. Cells were transfected with JetPRIME (Polyplus) with 10 μg plasmid DNA/500 μL Jet buffer/15 μL Jet reagent/petri dish. Two days post-transfection, cells were processed according to the GPCR purification protocol from Daulat *et al.* [33] suited for weak interactions including the interactions between G-proteins and their interactors, except that we collected also the cytoplasmic component. To do so, we replaced the long high-speed centrifugation with a simpler one of 800×*g* for 10 min at 4 °C. Briefly, cells were trypsinized, washed with cold PBS, and then lysed with the help of pistons for mechanical fragmentation. Then the lysates were solubilized by the addition of CHAPS detergent overnight at 4 °C. After centrifugation, supernatants were collected and left to interact with streptavidin beads for 4 h at 4 °C. After low-speed centrifugation, the supernatants were discharged and beads were washed. Then five elutions with D-biotin were performed to detach the proteins from the streptavidin beads. All collected supernatants were kept for 4 h at 4 °C with calmodulin beads supplemented with $CaCl_2$. After this incubation period, beads were washed without detergent. The final pellets were composed of calmodulin beads connected to the bait proteins; the connections were broken up by trypsinization and proteins submitted to mass spectrometry. For all experiments, three replicates were performed.

4.5. LC-MS/MS analysis

Samples were denatured, reduced, and alkylated in 100 ul 2% SDC, 40 mM Chloroacetamide, 10 mM TCEP, and 100 mM Tris HCl pH 8. Then samples were digested with 1 ug Trypsin overnight at 37 °C. After digestion beads were separated from the samples centrifuging for 5 min at 10,000 g and supernatants were processed by iST protocol [52]. The resulting peptides were analyzed by a nano-UHPLC-MS/MS system using an Ultimate 3000 RSLC coupled to an Orbitrap Fusion Tribrid mass spectrometer (Thermo Scientific Instrument). The samples were loaded from the sample loop directly into a 75-μm ID × 50 cm 2 μm, 100 Å C18 column, and peptides were separated with increasing organic solvent at a flow rate of 250 nl/min with a non-linear gradient of 7–45% solution B (80% ACN and 20% H2O, 5% DMSO, 0.1% FA) in 140 min. Orbitrap detection was used for MS1 measurements at resolving power of 120 K, while Ion Trap detection was used for MS2 measurements with Rapid Ion Trap Scan Rate as previously described [53]. MaxQuant software [54], version 1.6.6.0, was used to process the raw data, setting a false discovery rate (FDR) of 0.01 for the identification of proteins, peptides, and PSM (peptide-spectrum match), a minimum length of 6 amino acids for peptide identification was required. Andromeda engine, incorporated into MaxQuant software, was used to search MS/MS spectra against Uniprot human database (release UP000005640_9606 April 2019). In the processing, the variable modifications are Acetyl (Protein N-Term), Oxidation (M), Deamidation (NQ), on the contrary, the Carbamidomethyl (C) was selected as fixed modification. The intensity values were extracted and statistically evaluated using the ProteinGroup Table and Perseus software. Algorithm MaxLFQ was chosen for the protein quantification with the activated option 'match between runs' to reduce the number of the missing proteins. The mass spectrometry proteomics data have been deposited to the ProteomeXchange Consortium via the PRIDE [55] partner repository with the dataset identifier PXD030217.

4.6. Co-immunoprecipitation (Co-IP)

Immunoprecipitation was performed using a modification of the protocol described by Free *et al.* [56]. Briefly, OMM1 uveal melanoma cells (transfected with a mutated form of *GNAQ and GNA11)* were lysed (CHAPS IP buffer: 0.5% CHAPS, 150 mM NaCl, 1 mM EDTA, and protease inhibitor Roche) and washed once with cold PBS. Lysates were precleared with protein A/G Sepharose beads (Abcam) for 20 min. Control/mock IP was performed using an equal amount of lysate and mouse/rabbit isotype control IgG. IPs were performed at 4 °C with IP antibody, followed by 3 h of incubation in the presence of protein A/G Sepharose beads (Abcam). Beads were washed three times in IP buffer and, after addition of loading buffer, boiled at 90 °C for 5 min, centrifuged, resolved on pre-cast acrylamide gel (4/12% Bis-Tris), and transferred to nitrocellulose membranes (Life Sciences). Membranes were blocked

with 5% milk in TBST and probed with the primary antibody solution overnight at 4 °C. The following day, membranes were then incubated with the secondary antibody solution (polyclonal goat anti-rabbit or goat anti-mouse, Dako or VeriBlot for IP detection, Abcam) for 1 h at room temperature. Blots were imaged using a Uvitec imaging device (Cambridge, UK).

4.7. Statistical analysis

The metastatic risk by Kaplan–Meier survival analysis and Cox proportional hazard multiple regression model was tested as previously described [23]. The effects of the mutations on survival were assessed by the Kaplan–Meier survival analysis and the Mantel–Cox proportional hazard regression model; the log-rank and the Wald tests were used for significance assessments. The Fisher Exact test, the Mann–Whitney U test, and the Chi-square test were used in frequency and median comparisons as indicated in the legends. Calculations and plots were performed by using SPSS v.20. Statistical analysis for gene expression data was performed by using Significance Analysis of Microarray as previously described [23,57]. Gene enrichment analyses were executed by using EnrichR [58,59] and FunRich [60,61] tools.

Author Contributions

Francesca Piaggio FP performed in vitro experiments, wrote manuscript.

Michela Croce MC performed in vitro experiments.

Francesco Reggiani FR performed bioinformatics analysis.

Paola Monti PM performed in vitro experiments.

Cinzia Bernardi CB contributed to the design of the experimental plan.

Marianna Ambrosio MA performed in vitro experi ments.

Barbara Banelli BB contributed to the design of the experimental plan.

Mehmet Dogrusöz MD provided clinical information on UM patients and gene expression dataset.

Ralf Jockers RJ supervised TAP-MS experiments.

Domenico Bordo DB performed homology modelling analysis.

Roberto Puzone RP performed gene expression dataset preparation.

Silvia Viaggi SV critical revised manuscript.

Domenico Coviello DC critical revised manuscript.

Francesco B. Lanza FBL provided clinical information on UM patients.

Martina Bartolucci MB performed TAP-MS experi ments.

Andrea Petretto AP supervised TAP-MS experi ments.

Carlo Mosci CM provided clinical information on UM patients.

Rosaria Gangemi RG performed in vitro experiments, wrote manuscript, critical revised manuscript.

Pieter *A. van* der Velden PAV provided clinical information on UM patients.

Martine J. Jager MJ provided clinical information on UM patients, gene expression dataset and UM cell lines, critical revised manuscript.

Ulrich Pfeffer UP analyzed results, wrote manuscript and critical revised manuscript.

Adriana Amaro AA performed in vitro experiments, contributed to the design of the experimental plan wrote manuscript.

Funding

Our work is generously supported by the Italian Ministry of Health (5 × 1000 −2018−19) to AA, and by the Italian Ministry of Health (5 × 1000−2016) to MC and by the Italian Ministry of Health (Ricerca Corrente), Compagnia San Paolo, grant number 20067 and Associazione Italiana per la Ricerca sul Cancro, AIRC, grant number IG 17103 to UP, by the European Commission, through Horizon2020 UM CURE (667787) and Dutch cancer society (KWF) grant no UL2011-4991 to MJ, Federation of European Biochemical Societies (FEBS) Short Term Fellowship to FP.

Conflict of interest statement

The authors declare that they have no known competing financial interests or personal relationships that could have appeared to influence the work reported in this paper.

Acknowledgments

We thank Monica Fortin for project management. The results shown here are in part based upon data generated by the TCGA Research Network http://cancergenome.nih.gov/.

Appendix A. Supplementary data

Supplementary data to this article can be found online at https://doi.org/10.1016/j.ejca.2022.04.013.

References

[1] Chang AE, Karnell LH, Menck HR. The national cancer data base report on cutaneous and noncutaneous melanoma A summary of 84,836 cases from the past decade. 1998.

[2] Singh AD, Topham A. Incidence of uveal melanoma in the United States: 1973-1997. Ophthalmology 2003;110:956–61. https://doi.org/10.1016/S0161-6420(03)00078-2.

[3] Virgili G, Gatta G, Ciccolallo L, Capocaccia R, Biggeri A, Crocetti E, et al. Incidence of uveal melanoma in Europe. Ophthalmology 2007;114. https://doi.org/10.1016/J.OPHTHA.2007.01.032.

[4] Singh AD, Borden EC. Metastatic uveal melanoma. Ophthalmol Clin North Am 2005;18:143–50. ix. https://doi.org/S0896-1549(04)00086-0 [pii]10.1016/j.ohc.2004.07.003.
[5] Group* COMS. Development of metastatic disease after enrollment in the COMS trials for treatment of choroidal melanoma: collaborative ocular melanoma study group report No. 26. Arch Ophthalmol 2005;123:1639–43. https://doi.org/10.1001/ARCHOPHT.123.12.1639.
[6] Amaro A, Gangemi R, Piaggio F, Angelini G, Barisione G, Ferrini S, et al. The biology of uveal melanoma. Cancer Metastasis Rev 2017;36:109–40. https://doi.org/10.1007/s10555-017-9663-3.
[7] Jager MJ, Shields CL, Cebulla CM, Abdel-Rahman MH, Grossniklaus HE, Stern MH, et al. Uveal melanoma. Nat Rev Dis Prim 2020;6:1–25. https://doi.org/10.1038/s41572-020-0158-0.
[8] Rossi E, Croce M, Reggiani F, Schinzari G, Ambrosio M, Gangemi R, et al. Uveal melanoma metastasis. Cancers 2021;13:5684. https://doi.org/10.3390/CANCERS13225684. 2021;13:5684.
[9] Van Raamsdonk CD, Bezrookove V, Green G, Bauer J, Gaugler L, O'Brien JM, et al. Frequent somatic mutations of GNAQ in uveal melanoma and blue naevi. Nature 2009;457:599–602. https://doi.org/10.1038/nature07586.
[10] Van Raamsdonk CD, Griewank KG, Crosby MB, Garrido MC, Vemula S, Wiesner T, et al. Mutations in GNA11 in uveal melanoma. N Engl J Med 2010;363:2191–9. https://doi.org/10.1056/NEJMoa1000584.
[11] Dono M, Angelini G, Cecconi M, Amaro A, Esposito AI, Mirisola V, et al. Mutation frequencies of GNAQ, GNA11, BAP1, SF3B1, EIF1AX and TERT in uveal melanoma: detection of an activating mutation in the TERT gene promoter in a single case of uveal melanoma. Br J Cancer 2014;110:1058–65. https://doi.org/10.1038/bjc.2013.804.
[12] Onken MD, Worley LA, Long MD, Duan S, Council ML, Bowcock AM, et al. Oncogenic mutations in GNAQ occur early in uveal melanoma. Investig Ophthalmol Vis Sci 2008;49:5230–4. https://doi.org/10.1167/iovs.08-2145.
[13] Koopmans AE, Vaarwater J, Paridaens D, Naus NC, Kilic E, de Klein A, et al. Patient survival in uveal melanoma is not affected by oncogenic mutations in GNAQ and GNA11. Br J Cancer 2013;109:493–6. https://doi.org/10.1038/bjc.2013.299.
[14] Robertson AG, Shih J, Yau C, Gibb EA, Oba J, Mungall KL, et al. Integrative analysis identifies four molecular and clinical subsets in uveal melanoma. Cancer Cell 2018;33:151. https://doi.org/10.1016/j.ccell.2017.12.013.
[15] Markby DW, Onrust R, Bourne HR. Separate GTP binding and GTPase activating domains of a Gα subunit. Science 1993;262:1895. https://doi.org/10.1126/science.8266082. 901.
[16] O'Hayre M, Degese MS, Gutkind JS. Novel insights into G protein and G protein-coupled receptor signaling in cancer. Curr Opin Cell Biol 2014;27C:126–35. https://doi.org/10.1016/j.ceb.2014.01.005.
[17] Feng X, Degese MS, Iglesias-Bartolome R, Vaque JP, Molinolo AA, Rodrigues M, et al. Hippo-independent activation of YAP by the GNAQ uveal melanoma oncogene through a trio-regulated Rho GTPase signaling circuitry. Cancer Cell 2014;25:831–45. https://doi.org/10.1016/j.ccr.2014.04.016.
[18] Yu FX, Luo J, Mo JS, Liu G, Kim YC, Meng Z, et al. Mutant Gq/11 promote uveal melanoma tumorigenesis by activating YAP. Cancer Cell 2014;25:822–30. https://doi.org/10.1016/j.ccr.2014.04.017.
[19] Griewank KG, van de Nes J, Schilling B, Moll I, Sucker A, Kakavand H, et al. Genetic and clinico-pathologic analysis of metastatic uveal melanoma. Mod Pathol 2014;27:175–83. https://doi.org/10.1038/modpathol.2013.138.
[20] Staby KM, Gravdal K, Mørk SJ, Heegaard S, Vintermyr OK, Krohn J. Prognostic impact of chromosomal aberrations and GNAQ, GNA11 and BAP1 mutations in uveal melanoma. Acta Ophthalmol 2018;96:31–8. https://doi.org/10.1111/aos.13452.
[21] Wall MA, Coleman DE, Lee E, Iñiguez-Lluhi JA, Posner BA, Gilman AG, et al. The structure of the G protein heterotrimer Gi alpha 1 beta 1 gamma 2. Cell 1995;83:1047–58. https://doi.org/10.1016/0092-8674(95)90220-1.
[22] Herlihy N, Dogrusöz M, Van Essen TH, William Harbour J, Van Der Velden PA, Van Eggermond MCJA, et al. Skewed expression of the genes encoding epigenetic modifiers in high-risk uveal melanoma. Investig Ophthalmol Vis Sci 2015;56:1447–58. https://doi.org/10.1167/iovs.14-15250.
[23] Amaro A, Parodi F, Diedrich K, Angelini G, Götz C, Viaggi S, et al. Analysis of the expression and single-nucleotide variant frequencies of the butyrophilin-like 2 gene in patients with uveal melanoma. JAMA Ophthalmol 2016;134:1125–33. https://doi.org/10.1001/jamaophthalmol.2016.2691.
[24] Amaro A, Mirisola V, Angelini G, Musso A, Tosetti F, Esposito AI, et al. Evidence of epidermal growth factor receptor expression in uveal melanoma: inhibition of epidermal growth factor-mediated signalling by Gefitinib and Cetuximab triggered antibody-dependent cellular cytotoxicity. Eur J Cancer 2013;49:3353–65. https://doi.org/10.1016/j.ejca.2013.06.011.
[25] Robertson AG, Shih J, Yau C, Gibb EA, Oba J, Mungall KL, et al. Integrative analysis identifies four molecular and clinical subsets in uveal melanoma. Cancer Cell 2017;32:204–20. https://doi.org/10.1016/j.ccell.2017.07.003. e15.
[26] Koopmans AE, Verdijk RM, Brouwer RW, van den Bosch TP, van den Berg MM, Vaarwater J, et al. Clinical significance of immunohistochemistry for detection of BAP1 mutations in uveal melanoma. Mod Pathol 2014;27:1321–30. https://doi.org/10.1038/modpathol.2014.43.
[27] Scholz SL, Moller I, Reis H, Susskind D, van de Nes JAP, Leonardelli S, et al. Frequent GNAQ, GNA11, and EIF1AX mutations in Iris melanoma. Invest Ophthalmol Vis Sci 2017;58:3464–70.
[28] Van Essen TH, Van Pelt S, Versluis M, Bronkhorst IHG, Van Duinen SG, Marinkovic M, et al. Prognostic parameters in uveal melanoma and their association with BAP1 expression. Br J Ophthalmol 2014;98:1738–43. https://doi.org/10.1136/BJOPHTHALMOL-2014-305047.
[29] Patrone S, Maric I, Rutigliani M, Lanza F, Puntoni M, Banelli B, et al. Prognostic value of chromosomal imbalances, gene mutations, and BAP1 expression in uveal melanoma. Genes Chromosom Cancer 2018;57:387–400. https://doi.org/10.1002/gcc.22541.
[30] Shah AA, Bourne TD, Murali R. BAP1 protein loss by immunohistochemistry: a potentially useful tool for prognostic prediction in patients with uveal melanoma. Pathology 2013;45:651–6. https://doi.org/10.1097/PAT.0000000000000002.
[31] Piaggio F, Tozzo V, Bernardi C, Croce M, Puzone R, Viaggi S, et al. Secondary somatic mutations in g-protein-related pathways and mutation signatures in Uveal melanoma. Cancers (Basel) 2019;11. https://doi.org/10.3390/cancers11111688.
[32] Harbour JW. A prognostic test to predict the risk of metastasis in uveal melanoma based on a 15-gene expression profile. Methods Mol Biol 2014;1102:427–40. https://doi.org/10.1007/978-1-62703-727-3_22.
[33] Daulat AM, Maurice P, Froment C, Guillaume JL, Broussard C, Monsarrat B, et al. Purification and identification of G proteincoupled receptor protein complexes under native conditions. Mol Cell Proteomics 2007;6:835–44.
[34] Field MG, Kuznetsov JN, Bussies PL, Cai LZ, Alawa KA, Decatur CL, et al. BAP1 loss is associated with DNA methylomic repatterning in highly aggressive class 2 uveal melanomas. Clin Cancer Res 2019;25:5663–73. https://doi.org/10.1158/1078-0432.CCR-19-0366.
[35] Van Raamsdonk CD, Fitch KR, Fuchs H, De Angelis MH, Barsh GS. Effects of G-protein mutations on skin color. Nat Genet 2004;36:961–8. https://doi.org/10.1038/NG1412.

[36] Damato B, Dopierala J, Klaasen A, van Dijk M, Sibbring J, Coupland SE. Multiplex ligation-dependent probe amplification of uveal melanoma: correlation with metastatic death. Invest Ophthalmol Vis Sci 2009;50:3048–55. https://doi.org/iovs.08-3165 [pii]10.1167/iovs.08-3165.
[37] Kalirai H, Dodson A, Faqir S, Damato BE, Coupland SE. Lack of BAP1 protein expression in uveal melanoma is associated with increased metastatic risk and has utility in routine prognostic testing. Br J Cancer 2014;111:1373–80. https://doi.org/10.1038/bjc.2014.417.
[38] Naus NC, Verhoeven ACA, van Drunen E, Slater R, Mooy CM, Paridaens DA, et al. Detection of genetic prognostic markers in uveal melanoma biopsies using fluorescence in situ hybridization. Clin Cancer Res 2002;8.
[39] White VA, Chambers JD, Courtright PD, Chang WY, Horsman DE. Correlation of cytogenetic abnormalities with the outcome of patients with uveal melanoma. Cancer 1998;83:354–9. https://doi.org/10.1002/(SICI)1097-0142(19980715)83:2<354::AID-CNCR20>3.0.CO;2-R.
[40] de Lange MJ, van Pelt SI, Versluis M, Jordanova ES, Kroes WG, Ruivenkamp C, et al. Heterogeneity revealed by integrated genomic analysis uncovers a molecular switch in malignant uveal melanoma. Oncotarget 2015;6:37824–35. https://doi.org/10.18632/oncotarget.5637.
[41] Ehlers JP, Worley L, Onken MD, Harbour JW. DDEF1 is located in an amplified region of chromosome 8q and is overexpressed in uveal melanoma. Clin Cancer Res 2005;11:3609–13. https://doi.org/10.1158/1078-0432.CCR-04-1941.
[42] Biasini M, Bienert S, Waterhouse A, Arnold K, Studer G, Schmidt T, et al. SWISS-MODEL: modelling protein tertiary and quaternary structure using evolutionary information. Nucleic Acids Res 2014;42. https://doi.org/10.1093/NAR/GKU340.
[43] Waldo GL, Ricks TK, Hicks SN, Cheever ML, Kawano T, Tsuboi K, et al. Kinetic scaffolding mediated by a phospholipase C-beta and Gq signaling complex. Science 2010;330:974–80. https://doi.org/10.1126/SCIENCE.1193438.
[44] Dogrusöz M, Trasel AR, Cao J, Çolak S, van Pelt SI, Kroes WGM, et al. Differential expression of DNA repair genes in prognostically-favorable versus unfavorable uveal melanoma. Cancers (Basel) 2019;11. https://doi.org/10.3390/cancers11081104.
[45] Irizarry RA, Bolstad BM, Collin F, Cope LM, Hobbs B, Speed TP. Summaries of Affymetrix GeneChip probe level data. Nucleic Acids Res 2003;31:e15. https://doi.org/10.1093/nar/gng015.
[46] Irizarry RA, Hobbs B, Collin F, Beazer-Barclay YD, Antonellis KJ, Scherf U, et al. Exploration, normalization, and summaries of high density oligonucleotide array probe level data. Biostatistics 2003;4:249–64. https://doi.org/10.1093/biostatistics/4.2.249.
[47] Nannya Y, Sanada M, Nakazaki K, Hosoya N, Wang L, Hangaishi A, et al. A robust algorithm for copy number detection using high-density oligonucleotide single nucleotide polymorphism genotyping arrays. Cancer Res 2005;65:6071–9. https://doi.org/10.1158/0008-5472.CAN-05-0465.
[48] de Lange MJ, Razzaq L, Versluis M, Verlinde S, Dogrusoz M, Bohringer S, et al. Distribution of GNAQ and GNA11 mutation signatures in uveal melanoma points to a light dependent mutation mechanism. PLoS One 2015;10:e0138002. https://doi.org/10.1371/journal.pone.0138002.
[49] Ksander BR, Rubsamen PE, Olsen KR, Cousins SW, Streilein JW. Studies of tumor-infiltrating lymphocytes from a human choroidal melanoma. Invest Ophthalmol Vis Sci 1991;32:3198–208.
[50] De Waard-Siebinga I, Blom DR, Griffioen M, Schrier PI, Hoogendoorn E, Beverstock G, et al. Establishment and characterization of an uveal-melanoma cell line. Int J Cancer 1995;62:155–61. https://doi.org/10.1002/IJC.2910620208.
[51] Nareyeck G, Zeschnigk M, Bornfeld N, Anastassiou G. Novel cell lines derived by long-term culture of primary uveal melanomas. Ophthalmologica 2009;223:196–201. https://doi.org/10.1159/000201566.
[52] Kulak NA, Pichler G, Paron I, Nagaraj N, Mann M. Minimal, encapsulated proteomic-sample processing applied to copy-number estimation in eukaryotic cells. Nat Methods 2014;11:319–24. https://doi.org/10.1038/nmeth.2834.
[53] Marino A, Camponovo A, Degl'Innocenti A, Bartolucci M, Tapeinos C, Martinelli C, et al. Multifunctional temozolomide-loaded lipid superparamagnetic nanovectors: dual targeting and disintegration of glioblastoma spheroids by synergic chemotherapy and hyperthermia treatment. Nanoscale 2019;11:21227–48. https://doi.org/10.1039/C9NR07976A.
[54] Cox J, Mann M. MaxQuant enables high peptide identification rates, individualized p.p.b.-range mass accuracies and proteome-wide protein quantification. Nat Biotechnol 2008;26:1367–72. https://doi.org/10.1038/NBT.1511.
[55] Perez-Riverol Y, Csordas A, Bai J, Bernal-Llinares M, Hewapathirana S, Kundu DJ, et al. The PRIDE database and related tools and resources in 2019: improving support for quantification data. Nucleic Acids Res 2019;47:D442–50. https://doi.org/10.1093/NAR/GKY1106.
[56] Free RB, Hazelwood LA, Sibley DR. Identifying novel protein-protein interactions using co-immunoprecipitation and mass spectroscopy. Curr Protoc Neurosci 2009;Chapter 5:Unit 5.28. https://doi.org/10.1002/0471142301.ns0528s46.
[57] Tusher VG, Tibshirani R, Chu G. Significance analysis of microarrays applied to the ionizing radiation response. Proc Natl Acad Sci USA 2001;98:5116–21. https://doi.org/10.1073/pnas.091062498.
[58] Chen EY, Tan CM, Kou Y, Duan Q, Wang Z, Meirelles GV, et al. Enrichr: interactive and collaborative HTML5 gene list enrichment analysis tool. BMC Bioinf 2013;14. https://doi.org/10.1186/1471-2105-14-128.
[59] Kuleshov MV, Jones MR, Rouillard AD, Fernandez NF, Duan Q, Wang Z, et al. Enrichr: a comprehensive gene set enrichment analysis web server 2016 update. Nucleic Acids Res 2016;44:W90. https://doi.org/10.1093/nar/gkw377. 7.
[60] Pathan M, Keerthikumar S, Ang C-SS, Gangoda L, Quek CYJ, Williamson NA, et al. FunRich: An open access standalone functional enrichment and interaction network analysis tool 2015;15:2597–601.
[61] FunRich:: Functional enrichment analysis tool:: Home n.d. http://www.funrich.org/(accessed July 17, 2021).
[62] Maxime Meylan, Etienne Becht, Catherine Sautès-Fridman, Aurélien de Reyniès, Wolf H. Fridman, Florent Petitprez bioRxiv 2020.12.03.400754; doi: https://doi.org/10.1101/2020.12.03.400754.
[63] Becht E, Giraldo NA, Lacroix L, Buttard B, Elarouci N, Petitprez F, Selves J, Laurent-Puig P, Sautès-Fridman C, Fridman WH, de Reyniès A. Estimating the population abundance of tissue-infiltrating immune and stromal cell populations using gene expression. Genome Biol 2016 Oct 20;17(1):218. https://doi.org/10.1186/s13059-016-1070-5.
[64] Erratum in: Genome Biol. 2016 Dec 1;17(1):249. PMID: 27765066; PMCID: PMC5073889.